Journal Name

ARTICLE TYPE

Cite this: DOI: 10.1039/xxxxxxxxxx

Received Date
Accepted Date

DOI: 10.1039/xxxxxxxxxx

www.rsc.org/journalname

Evaluating Force Dependent Free Energy Profiles from the Splitting Probability†

Vishal Singh[a,b] and Parbati Biswas[a*]

Single molecule experiments have facilitated the investigation of the dynamics of conformational transitions of biomolecules. For the (un)folding transition of DNA hairpins, the theoretically calculated splitting probability from the generalized Langevin equation with a power-law frictional memory kernel exactly matches with that obtained from the experiments. The exact Potential of Mean Force (PMF) is calculated from the splitting probability using "committor inversion". The PMF of the selected DNA hairpin is also evaluated from the steered molecular dynamics (SMD) simulations with varying forces. SMD simulations clearly show that the conformational transitions of the DNA hairpin are a function of the pulling force. At lower forces, some conformational states are non-existent while, at higher forces all states are clearly demarcated in the free energy landscape. At higher forces, the unfolding rates are independent of the force, whereas at lower forces the rates increase linearly with the applied force. Force induced (un)folding of the biomolecule provides an insight to the dynamics of structural transitions through activated potential energy barriers.

1 Introduction

The dynamics of conformational transitions of biomolecules in solution may be described as a diffusion in a multidimensional free energy landscape (FEL) with many degrees of freedom[1–3]. This complex dynamics may be considerably simplified by projecting it onto a one-dimensional (1D) coordinate, assuming that the motion along all other coordinates are fast enough to be in thermal equilibrium[4,5]. Such a projection renders the barrier crossing dynamics non-Markovian[1,5], that may be monitored through a suitably chosen one-dimensional reaction coordinate. Typically, the end-to-end distance of the protein/nucleic acid is chosen as an appropriate reaction coordinate. The temporal evolution of this reaction coordinate may be correlated with the single-molecule experimental data. Single-molecule force spectroscopy (SMFS) and fluorescence resonance energy transfer (FRET) experiments are used to monitor the structural transitions of protein and nucleic acids both in equilibrium and non-equilibrium conditions under constant mechanical force to study the dynamics of folding/unfolding of these biomolecules[6–9]. The enhanced resolutions of the recent SMFS and FRET experiments upto a μs[10–12] have captured the motion of these biomolecules across the potential barrier through the "transition path" at the top of the barrier. Advances in the experimental techniques have been adequately complemented with parallel developments in both theory and simulations[3–5,13–15].

Conformational transitions of proteins and nucleic acids are intricately linked to their respective biological functions. Such transitions delineate the underlying free energy landscape of these biomolecules along a relevant reaction coordinate, where the energy of the molecule is depicted as a function of its all possible conformations. Thus, the free energy at equilibrium, $U(x)$, may be obtained from the logarithm of the probability distribution function, $p_{eq}(x)$, of the reaction coordinate, x, given by

$$U(x) = -k_B T \ln p_{eq}(x) \quad (1)$$

where, k_B is the Boltzmann constant and T is the absolute tem-

[a] Department of Chemistry, University of Delhi, Delhi 110007, India. [b] Delhi School of Public Health, Institution of Eminence, University of Delhi, Delhi-110007, India. *Tel: +911127666646; E-mail: pbiswas@chemistry.du.ac.in

† Electronic Supplementary Information (ESI) available: []. See DOI: 10.1039/b000000x/

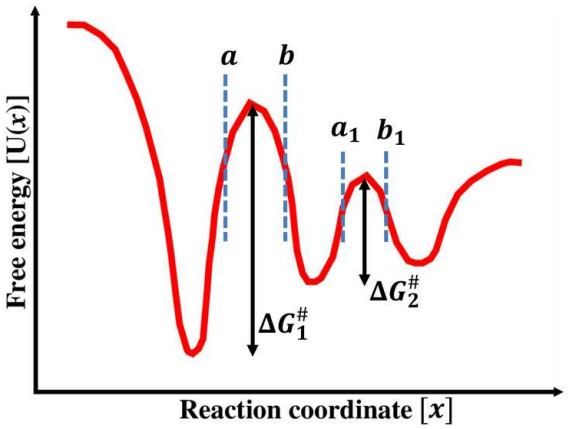

Fig. 1 Schematic potential energy for a three state system, where interval (a,b) (or (a_1,b_1)) is chosen in the barrier region and point x is defined in between the interval.

perature. This defines the Boltzmann inversion, which is only applicable at thermal equilibrium. However, for out-of equilibrium systems, the probability distribution may be defined through the splitting (committor) probability[3,5,6,16]. A point x is arbitrarily chosen within the barrier region (a,b) along the transition path. The splitting probability, $S_{p(a)}(x)/(S_{p(b)}(x) = 1 - S_{p(a)}(x))$ is defined as the probability of the trajectory that begins at x and crosses the boundary a/b without revisiting the other boundary b/a[3,5] (refer to Figure 1). Thus, for a symmetric potential well, the splitting probabilities are identical $S_{p(a)}(x) \approx S_{p(b)}(x) \approx 0.5$ in the limit $t_{max} \to \infty$[17], where t_{max} denotes the maximum time to reach one of the potential wells in the FEL. Splitting probability may be estimated from the folding trajectories of single molecules for a specified reaction coordinate x.

In this work, we aim to study the dynamics of the force induced conformational transitions of the DNA hairpin by evaluating the splitting probability and the potential of mean force (PMF). The rates of such transitions are also calculated in the limits of low and high forces. The theoretically calculated splitting probability evaluated from the overdamped generalized Langevin equation (GLE) with the non-Markovian frictional memory kernel matches with that of the experiments. Steered molecular dynamics (SMD) simulations of the selected hairpin are also performed at different pulling forces and the PMF is calculated using "committor inversion". From the simulations, it is clearly observed that the structural transitions of the DNA hairpin are a function of pulling force. At low forces, some states are less populated or unpopulated, while at higher forces, all states are populated and are clearly discernible. Thus, the force induced (un)folding of the biomolecule offers an insight to the dynamics of the conformational transitions of the DNA hairpin.

This article is organized as follows. The mathematical calculations of the splitting probabilities are given in Section 2. Section 3 provides the details of simulation of the DNA hairpin at different pulling forces. Results and discussions of both theory and the simulation results are compared and analyzed in Section 4 followed by the conclusions in Section 5.

2 Theory

The time evolution of the 1D reaction coordinate that governs the fold/unfold transition of the biomolecule in the complex cellular environment may be theoretically modeled via the overdamped generalized Langevin equation as[2,13,18–20]

$$m\int_0^t \gamma(t-t')\dot{x}(t')dt' + \frac{dU(x)}{dx} = \xi(t) \tag{2}$$

where the thermal fluctuations of the molecule are determined by the Gaussian random noise, $\xi(t)$, whose mean is defined by $\langle\xi(t)\rangle = 0$. The frictional memory kernel is related to the Gaussian-distributed random force by the fluctuation-dissipation theorem[18] as $\langle\xi(t)\xi(t')\rangle = k_BT\gamma(t-t')$, where the angular brackets denote statistical averaging over the noise ensemble. The conformational transitions of the DNA hairpin occur in a viscoelastic cellular medium, which introduces memory effects that makes the dynamics typically non-Markovian. This dynamics is modeled through a time-dependent power-law frictional memory kernel as $\langle\xi(t)\xi(0)\rangle = \frac{k_BT\eta_\beta t^{-\beta}}{\Gamma(1-\beta)}$. where, $\eta_\beta = \eta/\tau_c{}^{(1-\beta)}$ denotes the frictional coefficient and τ_c is the correlation time of the thermal fluctuations. The exponent β is a measure of the complexity of the cellular environment and may vary between 0 to 1 (i.e., $0 < \beta \leq 1$). While $\beta = 1$ shows a completely diffusive (homogeneous) environment, $\beta = 0$ corresponds to the heterogeneous surroundings. A generalized double well potential[13,19,21] for the conformational transitions of biomolecules is defined by

$$U(x) = 2k_BT\ln\ \Phi(A,x) \tag{3}$$

The term $\Phi(A,x)$ is represented as a linear combination of the even and odd solution of the Weber equation[13,21] with a biasing parameter, $(\mathscr{B})$. The simplified analytical expression of $\Phi(A,x)$ is given as

$$\begin{aligned}\Phi(A,x) &= y_1(A,x) + \mathscr{B}y_2(A,x)\\ &= exp\left(-\frac{k_S}{4k_BT}x^2\right)\left[{}_1F_1\left(\frac{A}{2}+\frac{1}{4},\frac{1}{2};\frac{k_S}{2k_BT}x^2\right)\right.\\ &\left.+\mathscr{B}x\sqrt{\frac{k_S}{k_BT}}{}_1F_1\left(\frac{A}{2}+\frac{3}{4},\frac{3}{2};\frac{k_S}{2k_BT}x^2\right)\right]\end{aligned} \tag{4}$$

where, k_s denotes the curvature of the energetic barrier that quantifies the rigidity of the optical trap and ${}_1F_1(\alpha,\beta;z)$ is the Kummer's (confluent hypergeometric) function. The values of A within $-1/2 \leq A < 0$ depict the depth of the potential well. The

biasing parameter $\mathscr{B}$ represents the symmetry of the well, with $\mathscr{B} = \sqrt{2}\frac{\Gamma(A/2+3/4)}{\Gamma(A/2+1/4)}$. While $\mathscr{B} < 0$ and $\mathscr{B} > 0$ represent the asymmetric bistable potential, $\mathscr{B} = 0$ denotes the symmetric potential.

The probability of finding the reaction coordinate, $x(t)$ of the biomolecule in the potential energy landscape at any time t is denoted by the conditional probability distribution, $P(x,t|x_0,t_0)$, assuming that the initial position of the molecule is x_0 at time $t = 0$ (t_0). Therefore, the effective Fokker-Planck equation (EFPE) may be recast in terms of $P(x,t|x_0,t_0)$ as (refer to Sections $1-3$ of the Supplementary Information)

$$\frac{\partial P(x,t|x_0,t_0)}{\partial t} = D(t)\left[\frac{\partial^2}{\partial x^2} + \frac{1}{k_BT}\frac{\partial}{\partial x}\frac{dU(x)}{dx}\right]P(x,t|x_0,t_0) \qquad (5)$$

where, $D(t) = \frac{k_BT}{k_S}\frac{\mathscr{Z}'(t)}{\mathscr{Z}(t)}$ denotes the time-dependent diffusion coefficient of the biomolecule in the complex cellular environment. The function $\mathscr{Z}$ is defined as; $\mathscr{Z} = E_{\beta,1}\left(D_\beta \frac{k_S}{k_BT}\, t^\beta\right)$, where, $E_{\beta,1}$ is the two-parameter Mittag-Leffler function and $D_\beta = \left(\frac{k_BT}{\eta_\beta}\right)$ $nm^2\mu s^{-\beta}$ is the diffusion coefficient in the cellular environment with varying heterogeneity of the medium. The conditional probability distribution, $P(x,t|x_0,t_0)$ may be obtained from the solution of Eqn. (5) as

$$P(x,t|x_0,t_0) = C_0^2\sqrt{\frac{k_S}{k_BT}}\frac{1}{(\Phi(A,x))^2} + \sum_{n=0}^{\infty} C_{n+1}^2\sqrt{\frac{k_BT}{k_S}}(\Phi(A,x_0))^2 \times \frac{d}{dx}\frac{D_n(x)}{\Phi(A,x)}\frac{d}{dx_0}\frac{D_n(x_0)}{\Phi(A,x_0)}\mathscr{Z}(t)^{-\left(n+A+\frac{1}{2}\right)} \qquad (6)$$

where, $D_n(x) = 2^{-n/2}exp\left(-ax^2/2\right)H_n(x\sqrt{a})$ is the cylindrical function and $H_n(x)$ is the Hermite polynomial. C_0 and C_{n+1} in Eqn. (6) are the normalization constants of the ground and excited states, respectively (refer to Sections 4 and 5 of the Supplementary Information).

Splitting probability of the biomolecule, $S_{p(x_A/x_B)}(x)$ at t_0 may be evaluated from $P(x,t|x_0,t_0)$. $S_{p(x_A/x_B)}(x)$, is defined as the zeroth moment of the first passage time distribution[15], $\mathscr{F}(x_0,t)$ between any two boundaries x_A and x_B, where, x_A and x_B correspond to the position of the left and right potential well in the FEL, respectively, $x_A < x(x_0) < x_B$ (refer to Figure 1; for the mathematical calculation, we use 'A' instead of 'a', whereas 'a' is used for the simulation calculations).

$$S_{p(x_A/x_B)}(x) = \int_0^\infty t^0\mathscr{F}(x_0,t)dt \qquad (7)$$

where, $\mathscr{F}(x_0,t)$ is expressed[20] as

$$\mathscr{F}(x_0,t) = -\frac{d}{dt}\int_{x_A}^{x_B} P(x,t|x_0,t_0)dx \qquad (8)$$

The splitting probability, $S_p(x)$, Eqn. (7) for a completely homogeneous (diffusive, $\beta = 1$) surroundings is obtained by substituting Eqn. (6) in Eqn. (8), as

$$S_{p(x_A/x_B)}(x) = D_1\sqrt{\frac{k_s}{k_BT}}(\Phi(A,x_0))^2\frac{1}{\sqrt{2\pi}}\int_0^\infty\sum_{n=0}^{\infty}\frac{1}{n!}\frac{d}{dx_0}\frac{D_n(x_0)}{\Phi(A,x_0)} \times \left[\frac{D_n(x)}{\Phi(A,x)}\right]\Bigg|_{x_A}^{x_B}\left[E_{1,1}\left(D_1\frac{k_s}{k_BT}t\right)\right]^{-(n+A+1/2)}dt \qquad (9)$$

3 Simulation Details

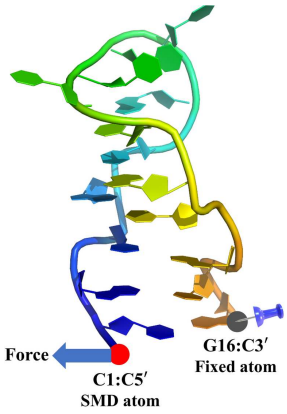

Fig. 2 Initial structure of the DNA hairpin (PDB ID:1D16). The unfolding of the hairpin are performed through SMD simulation at different pulling forces.

Implicit SMD simulations with appropriate force fields are also performed to calculate $S_p(x)$ and the corresponding PMF for the unfolding of T4 DNA hairpin with different pulling forces, f. Initial coordinate of the DNA hairpin is taken from Research Collaboratory for Structural Bioinformatics Protein Data Bank (RCSB PDB) with PDB ID: 1D16 (refer to Figures 2). The SMD simulations are performed implicitly for DNA hairpin using AMBER *leaprc.DNA.bsc*1 and *leaprc.DNA.OL*15 force fields[23] with NAMD-2.14 suite of programs[24]. Energy of each system is minimized to remove all unfavorable interactions in the molecules followed by raising the temperature to 300 K in two steps. Equilibration of the systems are done for 5 ns without using any periodic boundary conditions (PBC) and then multiple production runs at constant temperature (through Langevin thermostat[25]) are carried out for 20 ns to completely unfold the DNA. The Born radius cutoff for each atom is fixed to 12.0 Å. To unfold the DNA, constant force SMD simulations is performed by applying a constant force on $C5'$ atom of $C1$ residue, while fixing the $C3'$ atom of $G16$ residue of the hairpin. The SMD simulation of this molecule are carried out at different pulling forces (such as 1, 3, 5, 10, 14, 15, 18, and 25 pN) to study the dynamics of the multistate conformation tran-

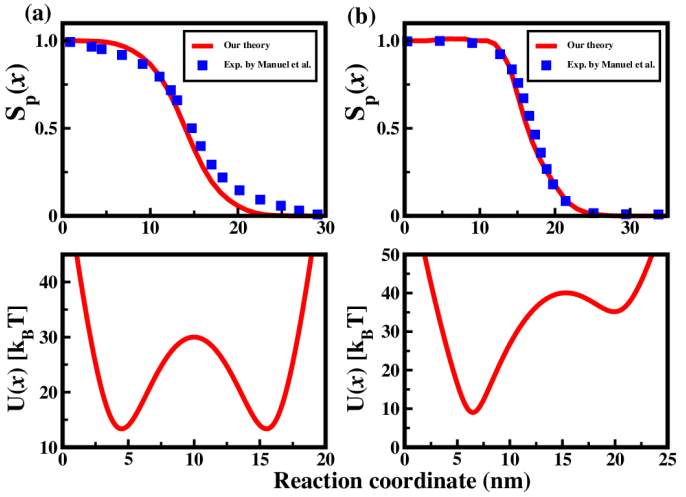

Fig. 3 Splitting probabilities for both (a) symmetric and (b) asymmetric bistable potentials calculated from Eqn. (9) and its corresponding free energy profiles. Splitting probabilitie for symmetric potential, the parameters are chosen as; $A=-0.44$ and $\mathscr{B}=0$ whereas, for asymmetric potential, the parameters are A=-0.44 and $\mathscr{B}=0.0717$. The other parameters are; $k_BT=16.54$ pN nm and $k_s=1.0$ pN nm^{-1}. For the calculation of $S_p(x)$ from the symmetric and asymmetric potentials, the experimental diffusion coefficients $D_1=0.1$ nm^2 μs^{-1} and $D_1=0.5$ nm^2 μs^{-1} are taken from the unfolding experiments of the DNA hairpins $20TS10/T4$ and $20TS06/T4$, respectively [22].

sition in the FEL. Here, the reaction coordinate is defined as the extension (i.e., the end-to-end distance between $C3'$ atom of $G16$ residue and $C5'$ atom of $C1$ residue) of the DNA.

4 Results and Discussions

For a simple two-state transition of the molecule in the conformational energy landscape across a potential barrier, $S_{p(x_B)}$ is zero ($S_{p(x_A)}\approx 1$) when the molecule lies in the left well, while $S_{p(x_B)}\approx 1$ for the other case. Figures 3(a) and 3(b) depict the splitting probabilities for both symmetric and asymmetric bistable potentials calculated from Eqn. (9) and its corresponding free energy profiles. For the symmetric potential, $S_p(x)$ is 0.5 at the transition state, which gives a sigmoidal curve. For the asymmetric potential, $S_p(x)$ deviates from this value as the (un)folding probability of the biomolecule changes along the reaction coordinate i.e. molecular extension and a non-sigmoidal curve is obtained. $S_p(x)$ calculated from theory (solid line) is compared with those obtained from experiments [6] (square symbol) for the folding hairpins $20TS10/T4$ and $20TS06/T4$ (refer to Figure 3). Here, $S_p(x)$ calculated from Eqn. (9) is in excellent agreement with those obtained from the experiments for both symmetric and asymmetric potentials.

The empirical splitting probability of the unfolding of the DNA hairpin may be directly estimated from the simulated trajectory of a finite duration, τ as [6,7,16]

$$S_p(x)=\frac{\int_0^\tau \delta(x-x(t))H_f(t)dt}{\int_0^\tau \delta(x-x(t))dt};\quad t\in[0,\tau]\ \&\ x\in[a,b] \tag{10}$$

where, H_f denotes the hitting function which monitors the simulation trajectory for a definite duration of time τ. The function $H_f(t)=1$ if the trajectory reaches a (folded state) just before b (unfolded state) just after time t, otherwise $H_f(t)=0$ (refer to Figure 1). Thus, the numerator of the above equation gives the number of trajectories that crosses x and reaches the boundary a before b and the denominator counts the total number of such crossings.

For a diffusive motion governed by the overdamped Langevin equation along x, the probability of $x\in[a,b]$ that hits the boundary a before b immediately is described by [3,5–7,16]

$$S_{p(a)}(x)=1-S_{p(b)}(x)=\frac{\int_x^b D^{-1}(x')e^{\beta U(x')}dx'}{\int_a^b D^{-1}(x')e^{\beta U(x')}dx'} \tag{11}$$

here, the coordinate independent diffusion coefficient is D and $\beta=1/k_BT$ is a measure of the thermal energy. Thus, the effective potential, $U(x)$, for any two-state conformational transition (i.e., folding/unfolding) may be calculated from Eqn. (11) as

$$U(x)=k_BT\ln\frac{dS_{p(a)}(x)}{dx} \tag{12}$$

This equation represents the generalized expression for the "committor inversion" which is used to reconstruct the PMF for the folding/unfolding transition of biomolecules and is independent of the friction coefficient. Thus, $S_p(x)$ encodes the free energy profile that quantifies the dynamics of such two-state transitions. The splitting probability profile depends on the strength of the pulling force.

The dynamics of the hairpin is extensively studied for different values of f ranging from low to high, as shown in Figure 4. $S_p(x)$ varies as a function of the pulling force f, applied at one end of the hairpin. Therefore, the shape of the PMFs and the curvature of the potential barrier for these conformational switches are also a function of f as it is directly derived from $S_p(x)$. At high forces, $f\geq 7$ pN, an intermediate state is populated in the conformational landscape between the fully folded and the unfolded state, which represents the three-state hairpin transition (Figure 4(b)). While, at low f (<7 pN), the hydrogen bonds between the guanine and cytosine base pairs of the T4 hairpin break slowly merging the intermediate state with the unfolded state resulting in a broad unfolded well. Therefore, only a two-state transition is observed in the conformational energy landscape for low pulling forces, which is further confirmed from the evaluation of the PDF (Figure 4(a)). This suggests that the conformational transitions of the DNA hairpins depend on the strength of the applied forces. For both cases, the native basin is found to be deeper and narrower

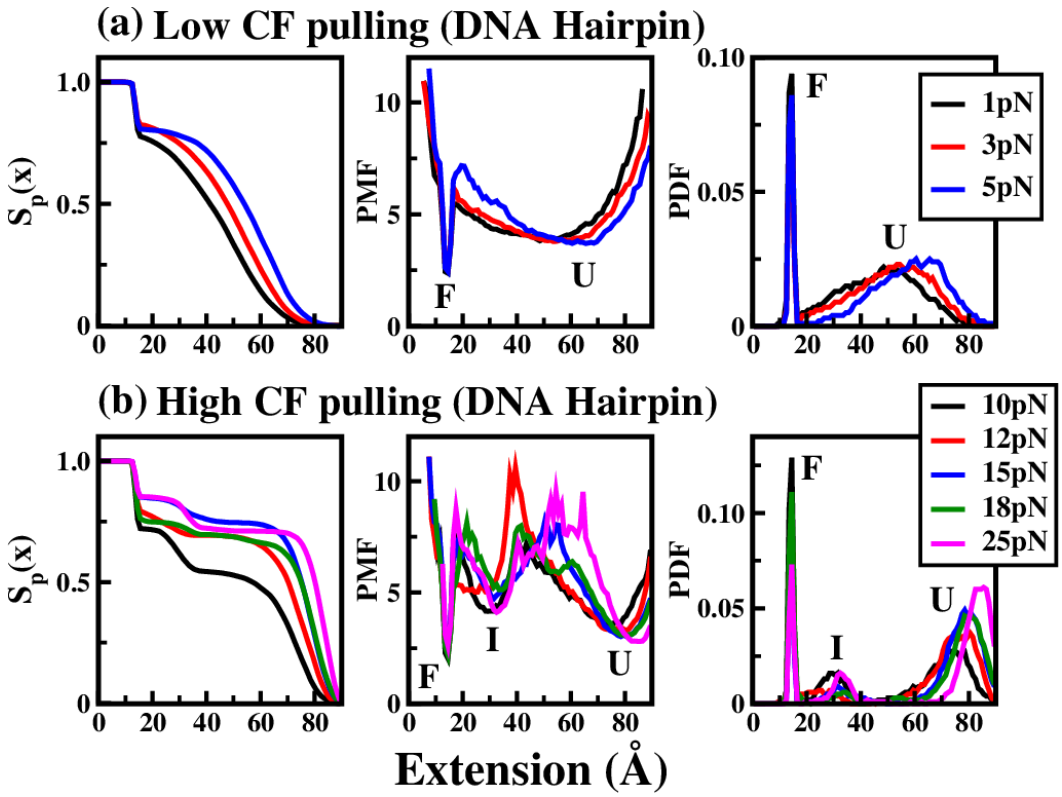

Fig. 4 Modulating the strength of f on one end of the DNA hairpin and the calculation of $S_p(x)$. Pulling at (a) low and (b) high constant forces (CF) show the two and three state conformational transitions of the hairpin, respectively which is further confirmed by analyzing the PMF and PDF from $S_p(x)$ data.

Force	$\overline{\tau}_{F\to I}$ (ns)	$k_{F\to I}$ (ns^{-1})	$\overline{\tau}_{I\to U}$ (ns)	$k_{I\to U}$ (ns^{-1})	$\overline{\tau}_{F\to U}$ (ns)	$k_{F\to U}$ (ns^{-1})
1 pN	–	–	–	–	0.14	7.14
2 pN	–	–	–	–	0.13	7.69
3 pN	–	–	–	–	0.12	8.33
5 pN	–	–	–	–	0.11	9.09
6 pN	–	–	–	–	0.10	10.00
10 pN	0.03 ± 0.00	37.44 ± 2.03	0.09 ± 0.01	13.21 ± 1.63	2.01 ± 0.09	0.53 ± 0.03
15 pN	0.05	20.00	0.07	14.28	1.49	0.67
18 pN	0.07	14.28	0.05	20.00	1.32	0.75
20 pN	0.08	13.33	0.05	20.00	1.20	0.83
25 pN	0.15	6.66	0.42	2.38	1.06	0.94

Table 1 Mean first passage time ($\overline{\tau}$) and the rate (k) for the conformational transition of DNA hairpin at different pulling forces. At lower forces, two-state transition is obtained, whereas, at higher forces a three-state hairpin transition is occurred in the FEL. Here, F, I and U denote the folded, intermediate and the unfolded state of the hairpin, respectively.

than the other potential well(s), which implies that the committor line at 0.5 is shifted towards the deeper well. Here, we also estimate the transition rates for the fold/unfold transition in the complex unfolding energy landscape of the hairpin ($F\to I\to U$) with varying f (refer to Table 1). The mean first passage time (MFPT, $\overline{\tau}$) for multiple distinct two-state transitions i.e. $F\to I$ and $I\to U$ (at higher f) and $F\to U$ (at lower f) is evaluated from the extension vs time simulation data, which is directly correlated to the rate of transitions as $k(f)=\overline{\tau}^{-1}(f)$. For an increase in the applied force at one end of the hairpin, the transition rate for $F\to I$ decreases and the potential barrier between F and I becomes sharper, which is committed towards both sides of the well. The rates of unfolding ($k_{F\to U}$) of T4 DNA hairpin at different low and high forces are shown in Figure 5 and Table 1. At low forces,

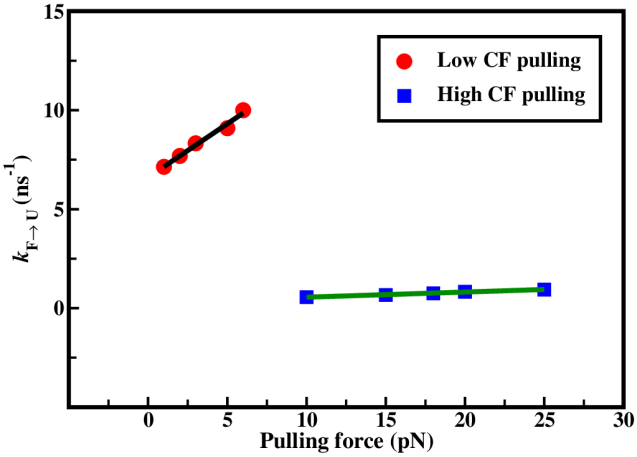

Fig. 5 Rate of unfolding versus pulling forces of the selected T4 DNA hairpin at low and high forces. At low forces, the unfolding rate is high, while at high forces, lower values of the rate is obtained.

$k_{F\to U}$ is much higher as compared to that at higher forces. Since, only folded and unfolded states of the hairpin are populated at low forces, therefore, the MFPT of unfolding of the hairpin is less resulting in a higher rate of transition. While, at high forces, an intermediate state is populated that lies in between the folded and unfolded states, which increases the MFPT of the unfolded state with a lower value of the unfolding rate. Also, in the low force regime, $k_{F\to U}$ increases linearly with pulling forces, whereas for higher forces, $k_{F\to U}$ practically remains constant.

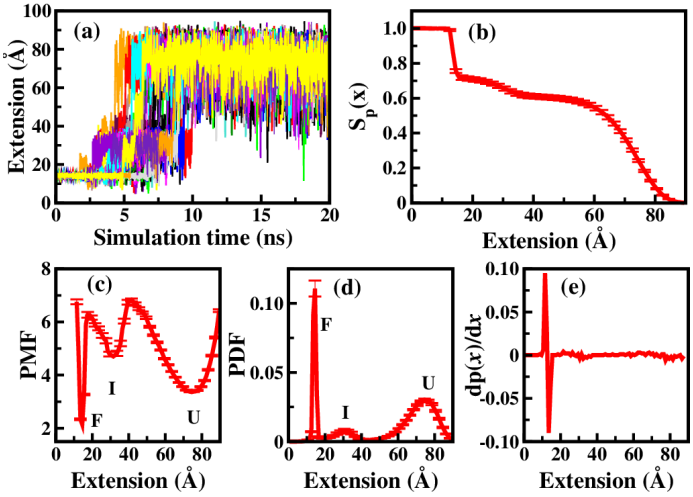

Fig. 6 SMD simulation of DNA hairpin at constant $f = 10$ pN. (a) Molecular extension versus simulation time plot shows for 50 independent trajectories which demonstrate three-state transitions of the hairpin. From these simulation data (b) $S_p(x)$ of these conformational changes are calculated. Other dynamical properties such as (c) PMF, (d) PDF and (e) first derivative of PDF are obtained directly from the calculated $S_p(x)$ that clearly show the three-state transitions. The error bars are calculated from 50 independent trajectories that begin with different initial velocities.

A total of 50 independent SMD simulations are performed at a constant force of $f = 10$ pN for the selected T4 DNA hairpin to investigate its dynamics. A three state transition of the hairpin is clearly observed from the simulation data (Figure 6(a)). Here, $S_p(x)$ is directly determined from the simulation data (Figure 6(b)) within the interval $[a,b]$ and the PMF is reconstructed (Figure 6(c)) from this probability using the committor inversion using Eqn. 12. Here, $S_p(x)$ is the combination of two non-sigmoidal curves which indicate three conformational states of the hairpin with unequal energy, which is reflected in its PMF profile. The apparent PMF calculated directly from the molecular trajectory provides inaccurate values of the barrier height[3,5], whereas the PMF obtained from $S_p(x)$ predicts an exact value of the height/curvature of the potential barrier. For this case, the height of the first free energy barrier, $\Delta G_1^{\ddagger} = 3.93$ kCal/mol and the second barrier is obtained at $\Delta G_2^{\ddagger} = 1.97$ kCal/mol, which confirms that the native/folded state of the hairpin is more stable than the other states, i.e. intermediate and the unfolded states, I and U. The first transition (i. e. $F \to I$) is considered as the rate limiting step for these conformational changes. The PDF of the unfolding of the hairpin also confirms that the native state is more populated and the intermediate state is the least populated at $f = 10$ pN (Figure 6(d)). The derivative of the probability distribution, $\dot{p}(x) = \frac{dp(x)}{dx}$ gives the exact location of the potential well and the number of transitions in the free energy landscape (Figure 6(e)).

5 Conclusions

In this study, we show that the free energy/PMF profile may be extracted from the splitting probability, which clearly shows that the conformational transitions are a function of the pulling force. The exact potential of mean force that determines the height and curvature of the potential barrier is calculated from the splitting probability using "committor inversion". The shape of the PMF changes by modulating the pulling forces applied at one end of the molecule along the reaction coordinate. At low forces, some states are less populated or unpopulated, while at higher forces, all states are populated and are clearly discernible. Thus, the dynamics of structural transitions of the DNA hairpin may be tuned by regulating the pulling force, which may be directly correlated to the free energy profile along an optimized reaction coordinate. Force induced (un)folding of the DNA hairpin provides an insight to the dynamics of structural transitions across activated energy barriers to their respective functionally active conformations.

Supplementary Information

See Supplementary Information for the solution of GLE under an asymmetric potential; conversion of the GLE to an effective Fokker-Planck equation; the solution of effective Fokker-Planck

equation; calculation of the normalization constants C_0 and C_{n+1}.

Conflicts of Interest

There are no conflicts to declare.

Acknowledgments

Vishal Singh acknowledges Delhi School of Public Health, Institution of Eminence (DSPH-IoE), University of Delhi for the financial support in form of a fellowship (IoE/2021/MKPDF/DSPH/143).

References

1 H. A. Kramers, *Physica*, 1940, **7**, 284–304.
2 R. Zwanzig, *Nonequilibrium Statistical Mechanics*, Oxford university press, New York, 2001.
3 D. E. Makarov, *J. Phys. Chem. B*, 2021, **125**, 2467–2476.
4 A. M. Berezhkovskii and A. Szabo, *J. Phys. Chem. B*, 2013, **117**, 13115–13119.
5 A. M. Berezhkovskii and D. E. Makarov, *J. Phys. Chem. Lett.*, 2020, **11**, 1682–1688.
6 A. P. Manuel, J. Lambert and M. T. Woodside, *Proc. Natl. Acad. Sci. U. S. A.*, 2015, **112**, 7183–7188.
7 J. D. Chodera and V. S. Pande, *Phys. Rev. Lett.*, 2011, **107**, 098102.
8 W. J. Greenleaf, K. L. Frieda, D. A. Foster, M. T. Woodside and S. M. Block, *Science*, 2008, **319**, 630–633.
9 K. Neupane, H. Yu, D. A. Foster, F. Wang and M. T. Woodside, *Nucleic Acids Res.*, 2011, **39**, 7677–7687.
10 H. S. Chung and W. A. Eaton, *Curr. Opin. Struct. Biol.*, 2018, **48**, 30–39.
11 N. Q. Hoffer and M. T. Woodside, *Curr. Opin. Struct. Biol.*, 2019, **53**, 68–74.
12 K. Neupane, D. A. Foster, D. R. Dee, H. Yu, F. Wang and M. T. Woodside, *Science*, 2016, **352**, 239–242.
13 S. Sharma, V. Singh and P. Biswas, *J. Chem. Phys.*, 2021, **154**, 185101.
14 V. Singh and P. Biswas, *J. Stat. Mech.: Theory Exp.*, 2021, **2021**, 063502.
15 W. K. Kim and R. R. Netz, *J. Chem. Phys.*, 2015, **143**, 224108.
16 R. Covino, M. T. Woodside, G. Hummer, A. Szabo and P. Cossio, *J. Chem. Phys.*, 2019, **151**, 154115.
17 G. Hummer, *J. Chem. Phys.*, 2004, **120**, 516–523.
18 R. Kubo, M. Toda and N. Hashitsume, *Statistical Physics II: Nonequilibrium Statistical Mechanics*, Springer-Verlag, Berlin, Heidelberg, 1985, vol. 31.
19 S. Sharma and P. Biswas, *J. Stat. Mech.: Theory Exp.*, 2020, **2020**, 073411.
20 S. Sharma, V. Singh and P. Biswas, *ACS Phys. Chem. Au*, 2022, **2**, 353–363.
21 M. O. Hongler and W. M. Zheng, *J. Math. Phys.*, 1983, **24**, 336–340.
22 K. Neupane, D. B. Ritchie, H. Yu, D. A. Foster, F. Wang and M. T. Woodside, *Phys. Rev. Lett.*, 2012, **109**, 068102.
23 R. Galindo-Murillo, J. C. Robertson, M. Zgarbova, J. Sponer, M. Otyepka, P. Jurecka and T. E. Cheatham III, *J. Chem. Theory Comput.*, 2016, **12**, 4114–4127.
24 J. C. Phillips, R. Braun, W. Wang, J. Gumbart, E. Tajkhorshid, E. Villa, C. Chipot, R. D. Skeel, L. Kale and K. Schulten, *J. Comput. Chem.*, 2005, **26**, 1781–1802.
25 W. F. Van Gunsteren and H. J. Berendsen, *Mol. Simul.*, 1988, **1**, 173–185.